SINGLE IMAGE SUPER-RESOLUTION VIA BM3D SPARSE CODING

Karen Egiazarian and Vladimir Katkovnik

Department of Signal Processing,Tampere University of Technology
Korkeakoulunkatu 10, 33720, Tampere, Finland, email: 'firstname.lastname'@tut.fi

ABSTRACT

In this paper, a novel single image super-resolution (SISR) algorithm is proposed. It is based on the BM3D (Block-Matching and 3D filtering) paradigm, where both sparsity and nonlocal patch self-similarity priors are utilized. The algorithm is derived from a variational formulation of the problem and has a structure typical for iterative back-projection super-resolution methods. They are characterized by updating high-resolution image which is calculated using the previous estimate and upsampled low-resolution error. The developed method is thoroughly compared with the state-of-the-art SISR both for noiseless and noisy data, demonstrating superior performance objectively and subjectively.

Index Terms— Single image super-resolution, sparse non-local imaging, image upsampling, image resizing

1. INTRODUCTION

Single image super-resolution (SISR) aims at constructing a high-resolution (HR) image from a single input low-resolution (LR) image. It is also known as an image interpolation or resizing. Classical interpolation methods, such as bilinear or bicubic, possess efficient implementation but resulting images suffer from visible over-smoothing. Iterative back-projection (IBP) methods [1], in opposite, may produce images with over-sharpened edges. Many image interpolation methods use IBP at their post-processing (edge sharpening) stage [2].

Super-resolution is an ill-posed problem and a regularization in the solution space is applied to it. This makes finding a good model of a prior of the target HR image to be extremely important. Various image priors have been used including global and local ones. Some global priors, like soft-edge and TV [3], [4] may result in images with overshooted edges. A sparsity prior has been applied in [2], [5], where coefficients of sparse representation of LR image patch have been used to produce the corresponding HR image patch.

Some recent SISR methods, including anchored neighborhood regression [6], [7] and deep-learning methods [8] based on principles of neighbor embedding and sparse coding, produce the state-of-the-art results. These learning-based methods are external, i.e. they use an external database of images to train the dictionary. Internal methods based on image self-similarity across the scales have been proposed in [9], [10].

In this paper, the problem of SISR is studied without any external dictionary. The proposed method, called SR-BM3D, is derived from the variational setting using a combination of self-semilarity, non-locality and sparsity priors coming from BM3D modeling [12]. It has a structural similarity to the back-projection (e.g. [1], [3], [11]) with two main differences: (1) filtering at each iteration is applied to HR images instead of filtering upsampled low-resolution errors (differences), and (2) the BM3D, image adaptive and very efficient denoising is applied for this filtering.

The paper is structured as follows. In Section 2, the proposed SR-BM3D algorithm is derived. Experimental results are given in Section 3 for noiseless and noisy data followed by the conclusion in Section 4.

2. SR-BM3D: ALGORITHM DERIVATION

2.1. Image formation and sparsity

Let the link between low- and high-resolution images be given in the form

$$\mathbf{x}_L = \mathbf{D}_s \mathbf{x}_H, \tag{1}$$

where $\mathbf{x}_L \in \mathbb{R}^m$, $\mathbf{x}_H \in \mathbb{R}^n$, $n > m$, and the matrix $\mathbf{D}_s \in \mathbb{R}^{m \times n}$ encodes blurring and downsampling transformations.

The scaling factor is defined as $s = n/m > 1$. The goal of SISR is to reconstruct the high-resolution $\mathbf{x}_H$ from the low-resolution observation $\mathbf{x}_L$ provided given $\mathbf{D}_s$. Recently, this problem appears in compressed sensing scenarios often including sparse modeling for $\mathbf{x}_H$ [15].

The equation (1) formalizes the problem at hand. Even if the focussing is precise and the optics - ideal, the downsampling formalized by the transform matrix $\mathbf{D}_s$ in practice never can be treated as a trivial subsampling. In particular, in a proper mathematical modeling, the downsampling assumes a continuous domain approximation of an image given on a high resolution grid and anti-aliasing filtering. Then, the matrix $\mathbf{D}_s$ is defined by the location of low and high resolution pixels, by the scale s, and by the applied interpolation method.

This work was supported in part by the Tekes, the Finnish Funding Agency for Technology and Innovation (Decision 40081/14, Dnro 338/31/2014, Parallel Acceleration Y2) and by Big Data project 83255 of-Tampere University of Technology

978-0-9928626-3-3/15/$31.00 ©2015 IEEE

Since the matrix $\mathbf{D}_s$ has far fewer rows than columns, SISR is an ill-posed inverse problem with an infinite number of solutions satisfying (1). Introducing an image prior is a standard way to overcome these uncertainness and to achieve an acceptable image quality.

In this paper, the sparsity of high-resolution image is used as a prior. We assume that $\mathbf{x}_H \in \mathbb{R}^n$ admits a sparse representation, or sparse coding, with respect to columns of a matrix $\mathbf{\Psi} \in \mathbb{R}^{n\times N}$; i.e. it is possible to write $\mathbf{x}_H = \mathbf{\Psi}\boldsymbol{\theta}$, where $\boldsymbol{\theta} \in \mathbb{R}^N$ is a vector containing only few non-zero components for a good approximation of $\mathbf{x}_H$. The matrix $\mathbf{\Psi}$ is termed as a synthesis operator (or dictionary). This synthesis representation for $\mathbf{x}_H$ has a dual point of view in which, given an image $\mathbf{x}_H \in \mathbb{R}^n$, its spectrum $\boldsymbol{\theta} \in \mathbb{R}^N$ is computed by applying the so-called analysis operator (or dictionary) $\mathbf{\Phi} \in \mathbb{R}^{N\times n}$ to $\mathbf{x}_H$, i.e. $\boldsymbol{\theta} = \mathbf{\Phi}\mathbf{x}_H$. The requirement of the perfect analysis-synthesis reconstruction means that $\mathbf{\Psi}\mathbf{\Phi} = \mathbf{I}_n$, where $\mathbf{I}_n$ is the $n \times n$ identity matrix. It happens, that when we are looking for sparsest approximations, the likelihood of success increases for overcomplete transforms with $N \gg n$. The concept of a frame is an important generalization of the classical bases especially developed for overcomplete (synthesis and analysis) representations with linearly dependent approximating functions. The success of the sparse imaging strongly depends on how rich and redundant are the analysis and synthesis dictionaries. For sparse modeling of $\mathbf{x}_H$ the analysis and synthesis BM3D frames developed in [13] are used. These frames belong to the class of the 'internal' transforms (dictionaries) extracted from the given observations. The efficiency of these transforms for image sparse modeling is confirmed by successive use of the BM3D filters.

2.2. Optimization

A sparse reconstruction of $\mathbf{x}_H$ can be formulated as the following optimization problem:

$$\min_{\theta\in\mathbb{R}^N} J,\ J = \frac{1}{2}||\mathbf{x}_L - \mathbf{D}_s\mathbf{x}_H||_2^2 + \tau_\theta||\boldsymbol{\theta}||_0, \quad (2)$$
$$\mathbf{x}_H = \mathbf{\Psi}\boldsymbol{\theta},$$

where the first summand in J is the Euclidean norm of the residuals (1); the second summand is a regularization term (penalization) enabling the sparsity of $\mathbf{x}_H$. Recall that l_0-pseudo norm, $||\boldsymbol{\theta}||_0$, is calculated as a number of nonzero elements of $\boldsymbol{\theta}$. Thus, smaller $||\boldsymbol{\theta}||_0$ corresponds to a sparser representation for $\mathbf{x}_H$. While the straightforward minimization (2) is possible, our approach is essentially different. Following [13], we apply the multiple-criteria Nash equilibrium technique [14]. In this approach both the synthesis $\mathbf{\Psi}$ and analysis $\mathbf{\Phi}$ transforms are exploited, contrary to (2) where the synthesis transform is used only.

Let us introduce the following three criteria:

$$J_1(\boldsymbol{\theta}, \mathbf{x}_H) = \frac{1}{2}||\boldsymbol{\theta} - \mathbf{\Phi}\mathbf{x}_H||_2^2 + \tau_\theta||\boldsymbol{\theta}||_0 \quad (3)$$
$$J_2(\hat{\mathbf{x}}_L, \boldsymbol{\theta}) = \frac{1}{2}||\mathbf{x}_L - \hat{\mathbf{x}}_L||_2^2 + \frac{1}{2\gamma_1}||\hat{\mathbf{x}}_L - \mathbf{D}_s(\mathbf{\Psi}\boldsymbol{\theta})||_2^2,$$
$$J_3(\mathbf{x}_H, \hat{\mathbf{x}}_L) = \frac{1}{2}||\hat{\mathbf{x}}_L - \mathbf{D}_s\mathbf{x}_H||_2^2 + \frac{1}{2\gamma_2}||\mathbf{x}_H||_2^2.$$

The criterion J_1 enables the sparsity of the spectrum $\boldsymbol{\theta}$ for $\mathbf{x}_H$. The $\hat{\mathbf{x}}_L$ is an auxiliary splitting variable making the multi-criteria approach much more manageable in comparison with the single criterion approach based on (2). While $\mathbf{x}_L$ is a given low-resolution observation, $\hat{\mathbf{x}}_L$ is an estimate of $\mathbf{x}_L$. In J_2 we have two quadratic summands calculated as the Euclidean norm of the error between $\mathbf{x}_L$ and $\hat{\mathbf{x}}_L$ and between $\hat{\mathbf{x}}_L$ and the prediction for $\mathbf{x}_L$ obtained from the high-resolution spectrum $\boldsymbol{\theta}$ using the synthesis transform $\mathbf{\Psi}$ and downsampling $\mathbf{D}_s$. J_3 formalizes the upsampling of $\mathbf{x}_L$ to $\mathbf{x}_H$ as an inverse problem with the quadratic regularization. The Nash equilibrium for (3) is a consensus of restrictions imposed by J_1, J_2, J_3 defined as a fixed point ($\boldsymbol{\theta}^*$,$\mathbf{x}_L^*$, $\mathbf{x}_H^*$) such that:

$$\boldsymbol{\theta}^* = \arg\min_{\boldsymbol{\theta}} J_1(\boldsymbol{\theta}, \mathbf{x}_H^*),\ \hat{\mathbf{x}}_L^* = \min_{\hat{\mathbf{x}}_L} J_2(\hat{\mathbf{x}}_L, \boldsymbol{\theta}^*), \quad (4)$$
$$\mathbf{x}_H^* = \min_{\mathbf{x}_H} J_3(\mathbf{x}_H, \hat{\mathbf{x}}_L^*).$$

If the equilibrium ($\boldsymbol{\theta}^*$,$\hat{\mathbf{x}}_L^*$, $\mathbf{x}_H^*$) exists, any deviation from it results in increasing of at least one of the criteria. If l_0-pseudo norm in J_1 is replaced by l_1-norm, calculated as the sum of the absolute values of the vector, then all the criteria in (3) are convex and the fixed point (4) exists under quite mild constrains. While this sort of results are unknown for l_0, the experiments show that the algorithm based on l_0 pseudo-norm performs better than that for l_1-norm.

The iterative algorithm looking for the fixed point has the following conventional iterative form [14]:

$$\boldsymbol{\theta}^k = \arg\min_{\boldsymbol{\theta}} J_1(\boldsymbol{\theta}, \mathbf{x}_H^k),\ \hat{\mathbf{x}}_L^{k+1} = \min_{\hat{\mathbf{x}}_L} J_2(\hat{\mathbf{x}}_L, \boldsymbol{\theta}^k), \quad (5)$$
$$\mathbf{x}_H^{k+1} = \min_{\mathbf{x}_H} J_3(\mathbf{x}_H, \hat{\mathbf{x}}_L^{k+1}),\ k = 0, 1, ... \quad (6)$$

The solution of the first problem in (5) is the hard thresholding with the threshold equal to $\sqrt{2\tau_\theta}$:

$$\boldsymbol{\theta}^k = Th_{\sqrt{2\tau_\theta}}(\mathbf{\Phi}\mathbf{x}_H^k). \quad (7)$$

The solution of the second quadratic problem in (5) is of the form:

$$\hat{\mathbf{x}}_L^{k+1} = (\mathbf{x}_L + \frac{1}{\gamma_1}\mathbf{D}_s(\mathbf{\Psi}\boldsymbol{\theta}^k))/(1 + 1/\gamma_1). \quad (8)$$

The solution of the third problem (5) defines the upsampling as the regularized inverse operator:

$$\mathbf{x}_H^{k+1} = (\mathbf{D}_s^T\mathbf{D}_s + \mathbf{I}_N/\gamma_2)^{-1}\mathbf{D}_s^T\hat{\mathbf{x}}_L^{k+1}. \quad (9)$$

Straightforward manipulations allow to rewrite (8) in the form

$$\hat{\mathbf{x}}_L^{k+1} = \tilde{\mathbf{x}}_L^k + \beta(\mathbf{x}_L - \tilde{\mathbf{x}}_L^k),\ \tilde{\mathbf{x}}_L^k = \mathbf{D}_s\mathbf{x}_H^k, \qquad (10)$$

where $\mathbf{x}_H^k = \boldsymbol{\Psi}\boldsymbol{\theta}^k$ is a high-resolution image after BM3D filtering and $\beta = \gamma_1/(1+\gamma_1), 0 < \beta < 1$.

Inserting (10) to (9), we obtain:

$$\mathbf{x}_H^{k+1} = (\mathbf{D}_s^T\mathbf{D}_s + \mathbf{I}_N/\gamma_2)^{-1}\mathbf{D}_s^T\mathbf{D}_s\mathbf{x}_H^k + \beta(\mathbf{D}_s^T\mathbf{D}_s + \mathbf{I}_N/\gamma_2)^{-1}\mathbf{D}_s^T(\mathbf{x}_L - \tilde{\mathbf{x}}_L^k)) \simeq \mathbf{x}_H^k + \beta\mathbf{U}_s(\mathbf{x}_L - \tilde{\mathbf{x}}_L^k). \qquad (11)\ (12)$$

Here $\mathbf{U}_s = (\mathbf{D}_s^T\mathbf{D}_s + \mathbf{I}_N/\gamma_2)^{-1}\mathbf{D}_s$ is an upsampling matrix, and it is assumed that $(\mathbf{D}_s^T\mathbf{D}_s + \mathbf{I}_N/\gamma_2)^{-1}\mathbf{D}_s^T\mathbf{D}_s\mathbf{x}_H^k \simeq \mathbf{x}_H^k$, i.e. the upsampling $\mathbf{U}_s$ nearly compensates the downsampling $\mathbf{D}_s$ for $\mathbf{x}_H^k$.

2.3. Proposed Algorithm

It can be verified using [13] that for the given BM3D frames $\boldsymbol{\Phi}$ and $\boldsymbol{\Psi}$ the solution (7) and the equation $\mathbf{x}_H^k = \boldsymbol{\Psi}\boldsymbol{\theta}^k$ are precisely correspond to the hard thresholding stage of the BM3D filter [12]. Using this fact and (12), we arrive to the two-stage iterative algorithm shown in Table 1.

Table 1. SR-BM3D Algorithm

Input:	x_L, s, D_s, U_s, x_H^0;
Output:	$\hat{x}_H^M$;
For:	$k = 0, 1, .., M-1$,
Stage 1:	$\hat{x}_H^k = BM3D(\hat{x}_H^k, \tau_\theta)$,
Stage 2:	$\hat{x}_H^{k+1} = \hat{x}_H^k + \beta U_s(x_L - D_s(\hat{x}_H^k))$.

The algorithm is described using standard 2D image variables (instead of vector notations used above). Here, D_s and U_s are down- and upsampling image domain operators defined above by the corresponding matrices. $BM3D(\hat{x}_H^k, \tau_\theta)$ is the BM3D filter applied to the high-resolution image estimate $\hat{x}_H^k$ with the hard thresholding parameter τ_θ. The frames $\boldsymbol{\Phi}$, $\boldsymbol{\Psi}$ are not shown because they are hidden inside of the BM3D filter.

3. EXPERIMENTAL RESULTS

Two notes concerning the algorithm implementation for our experiments are of importance. First, for downsampling D_s in Stage 2 we use the MATLAB's bicubic imresize function. By default, the downsampling matrix $\mathbf{D}_s$ is defined by this function and depends of the used interpolation method. Respectively, we replace the upsampling operator in (12) by this MATLAB's function used in the upsampling mode, in particular, because the downsampling matrix $\mathbf{D}_s$ is unknown explicitly for the downsampling defined by this imresize function.

Second, the standard BM3D filter [12] has two successive stages. The first is the hard thresholding filtering and the second one is the empirical Wiener filtering. The derivation of our algorithm leads to the BM3D with the single hard thresholding stage. Our experiments have demonstrated that using two stage BM3D with the Wiener filtering allows to improve the results. Thus, in what follows, we show results for two stage BM3D filter.

In this section, we provide experimental results of SISR and demonstrate the superiority of the proposed algorithm comparing to the state-of-the-art. Qualitative and quantitative evaluations are performed adopting the testing benchmarks of several recent SISR methods, including ANR [6], A+ [7], Yang [2], Zeyde [5], and others.

The following image databases have been used for testing [6] : 'Set5' , 'Set14', 'B100', where images have been downsampled by factors 2, 3 and 4, using 'bicubic' resizing kernel to form input low-resolution images. The quantitative evaluation is done by PSNR values measured on the luminance channel similarly as it is done in the cited publications and SSIM.

The following parameter settings are used in our experiments:

- parameter β is set to 1.75;

- CBM3D (Color BM3D) filter is used at each iteration (overall 40 iterations) in two stages: hard thresholding and Wiener filtering. For the hard thresholding stage of CBM3D: color space transform - 'YCbCr'; patch size is 8x8; shift to the next patch by 7; maximum number of similar patches - 16; macro block for a search - 29; transform used - 2D DCT + 1D Haar. For the Wiener filtering stage of CBM3D: color space transform - 'Opponent' (3-point DCT); patch size - $2s$ (s is the scaling factor); shift by $2s-2$; maximum number of similar patches - 32; macroblock search area - 39; transforms used 2D identity + 1D Haar.

- the threshold parameter for Color BM3D (CBM3D) filter is varying in iterations as a quadratic function decreasing from $12s$ to s.

As we can see from Table 2, the proposed approach outperforms the state-of-the-art $A+$ algorithm by a good margin. For visual comparison in Figures 1-2 we show examples of super-resolved images by the proposed algorithm and some competitors: true image (a), bicubic (b), A+ algorithm (c), proposed algorithm (d). These examples demonstrate better visual appearance of images generated by our method, edges and details appear less blurry and much clearer than those produced by other methods. Figure 3 shows examples of SISR applied to noisy input LR images, outperforming state-of-the-art [16] by more than 1 db. The difference between the noisy and noise-free SR-BM3D is that a low-resolution image x_L in Stage 2 of the SR-BM3D algorithm is replaced by the BM3D pre-filtered x_L.

Table 2. Average PSNR (dB)/SSIM (x100) for upscaling factors x2, x3 and x4 for Set5, Set14 and B100 datasets

Dataset	Scale	Bicubic	Zeyde	GR	ANR	A+	SR-BM3D
Set5	x2	33.7 / 93.0	35.8 / 94.9	35.1 / 94.4	35.8 / 95.0	36.6 / 95.4	**37.1 / 96.8**
	x3	30.4 / 86.8	31.9 / 89.7	31.4 / 88.4	31.9 / 89.7	32.6 / 90.9	**33.3 / 91.7**
	x4	28.4 / 81.1	29.7 / 84.4	29.3 / 82.8	29.7 / 84.3	30.3 / 86.1	**31.0 / 87.6**
Set14	x2	30.2 / 86.8	31.8 / 89.9	31.7 / 89.7	31.8 / 90.0	32.3 / 90.5	**32.8 / 90.8**
	x3	27.5 / 77.3	28.7 / 80.7	28.3 / 80.3	28.7 / 80.9	29.1 / 81.8	**29.6 / 82.5**
	x4	26.0 / 70.1	26.9 / 73.3	26.6 / 72.7	26.9 / 73.5	27.3 / 74.8	**27.7 / 75.8**
B100	x2	29.3 / 83.3	30.4 / 86.8	30.2 / 87.0	30.4 / 87.1	30.8 / 87.7	**31.5 / 87.9**
	x3	27.2 / 73.5	27.9 / 76.8	27.7 / 76.9	27.9 / 77.2	28.2 / 78.0	**28.5 / 78.4**
	x4	25.9 / 66.6	26.5 / 69.5	26.4 / 69.4	26.5 / 69.8	26.8 / 70.7	**27.0 / 71.3**

4. CONCLUSION

The variational technique was proposed for derivation of the SR-BM3D algorithm. Two important aspects define its difference from the conventional back-projection SISR method. First, at every iteration an updated HR image is filtered, while in the conventional back-projections algorithm a Gaussian filtering is applied to the upsampled low-resolution residuals. Second, the BM3D filtering derived from the variational setting of the problem was used. The developed algorithm was thoroughly compared with the current state-of-the-art algorithms for noiseless data. The proposed SR-BM3D algorithm using the internal dictionary image modeling has demonstrated better performance than the methods based on much more computationally demanding external dictionaries. The developed approach was also extended to the case of noisy observations again outperforming existed methods.

REFERENCES

[1] M. Irani and S. Peleg, “Motion analysis for image enhancement: resolution, occlusion and transparency,” *Journal of Visual Commun. and Image Representation*, Vol. 4, No. 4, pp. 324-335, 1993.

[2] J. Yang, J. Wright, T. Huang, and Y. Ma, "Image super-resolution via sparse representation", *IEEE Trans. on Image Processing,* vol. 19, pp. 2861-2873, 2010.

[3] S. Y. Dai, M. Han, W. Xu, Y. Wu, and Y. H. Gong, “Soft edge smoothness prior for alpha channel super resolution,” in *Proc. CVPR*, pp. 1–8, 2007.

[4] H. A. Aly and E. Dubois, “Image up-sampling using total-variation regularization with a new observation model,” *IEEE Trans. Image Process*, vol. 14, no. 10, pp.1647–1659, 2005.

[5] R. Zeyde, M. Elad and M. Protter, ”On Single Image Scale-Up Using Sparse Representations,” *Curves and Surfaces*, pp. 711–730, 2012.

[6] R. Timofte, V. De Smet and L.Van Gool, ”Anchored neighborhood regression for fast example-based super-resolution,” *Proc. IEEE Int. Conf. on Computer Vision.*, pp. 1920–1927, 2013.

[7] R. Timofte, V. De Smet, and L. Van Gool. "A+: Adjusted anchored neighborhood regression for fast super-resolution,” *Asian Conf. on Computer Vision (ACCV 2014)*, 1-5 November 2014.

[8] C. Dong, C.C. Loy, K. He, and X. Tang, ”Learning a deep convolutional network for image super-resolution,” *European Conf. on Computer Vision (ECCV 2014)*, pp. 184–199, 2014.

[9] D. Glasner, S. Bagon and M. Irani, "Super-resolution from a single image", In: *Proc. IEEE Int. Conf. on Computer Vision*, 2009.

[10] G. Freedman and R. Fattal, "Image and video upscaling from local self-examples", *ACM Trans. on Graphics* 30, pp. 12:1 12:11, 2011.

[11] S. Dai, M. Han, Y. Wu, and Y. Gong, ”Bilateral back-projection for single image super resolution,” *IEEE Conf. on Mult. and Expo, ICME*, pp. 1039-1042, 2007.

[12] K. Dabov, A. Foi, V. Katkovnik, and K. Egiazarian, “Image denoising by sparse 3D transform-domain collaborative filtering”, *IEEE Trans. Image Process.*, vol. 16, no. 8, pp. 2080-2095, 2007.

[13] A. Danielyan, V. Katkovnik and K. Egiazarian, “ BM3D frames and variational image deblurring, ” *IEEE Trans. Image Process*. 21 , pp. 1715 – 1728, 2012.

[14] F. Facchinei and C. Kanzow, “Generalized Nash equilibrium problems,” *4OR: A Quarterly Journal of Operations Research*, vol. 5, pp. 173–210, 2007.

[15] C. Fernandez-Granda, “Super-resolution and Compressed Sensing,” *SIAM News*, vol. 46, no. 8, October 2013

[16] A. Singh, F. Porikli, N. Ahuja, “Super-resolving noisy images,” *CVPR*, IEEE Conference on Computer Vision and Pattern Recognition, 23-28 June 2014, pp. 2846 - 2853.

Fig. 1. Cropped 'Butterfly' image from Set5 with upscaling x4. From left to right: original HR image; result of bicubic interpolation PSNR=21.1 dB;, A+ super-resolution PSNR=24.4 dB; super-resolution by SR-BM3D PSNR=26.1 dB.

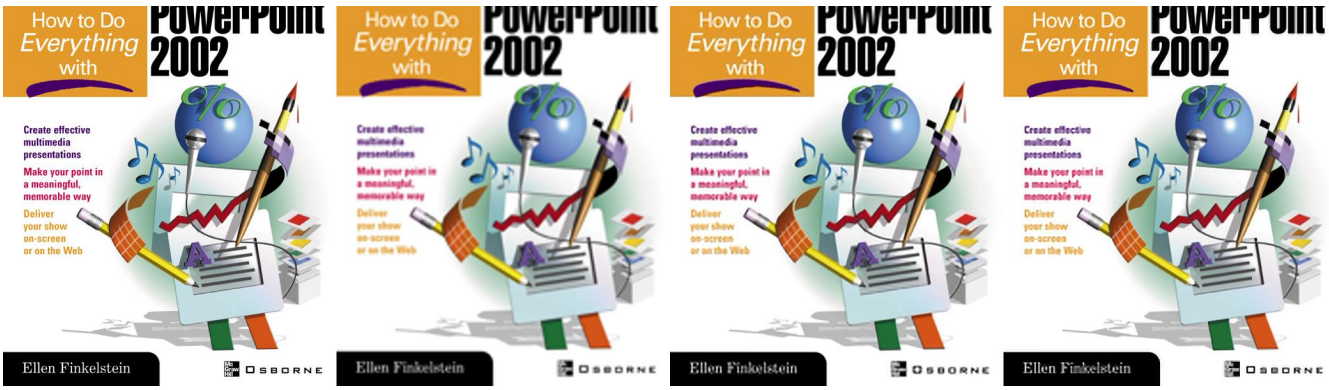

Fig. 2. Cropped 'ppt3' image from Set14 with upscaling x3. From left to right: original HR image; result of bicubic interpolation PSNR=23.7 dB; A+ super-resolution PSNR=26.1 dB; super-resolution by SR-BM3D PSNR=27.3 dB.

Fig. 3. Noisy LR images 'horses' (additive white Gaussian noise, sigma = 25) and 'dog' (sigma = 20) and results of SR-BM3D ('horses': PSNR = 25.27 db/SSIM = 0.664; 'dog': PSNR = 29.46 db/SSIM = 0.776) with upscaling x2